MODELLING OF SOIL PROFILE POLLUTANT YIELD ON SLAUGHTERHOUSE WASTES DEPOSITED LAND.

ABSTRACT

Aim: The study aimed at modelling the concentration of pollutants along soil profile using finite element method.

Study Design: Data was generated from the laboratory on the concentrations of selected heavy metals at varying depths of land discharged slaughterhouses. This was used to estimate the level of nutrient build-up in the soil within these environs, hence, used to verify and validate the finite element developed model. The model upon validation was used to predict the rate of pollutant build-up in the soil within the slaughterhouses discharge areas.

Methodology: A total of twelve composite samples were collected from three different land discharged locations. The three composite samples each were collected from the sampling locations at a depth of 0 to 10cm, 10 to 20cm, 20 to 30cm and 30 to 40cm. Four composite samples each were collected for analysis from the three sampling locations on specified sampling dates. The samples were then placed in sterile polythene bags and transported to the laboratory for processing. The laboratory results obtained for heavy metals were used for the generated model verification and validation, hence predictions for pollutants accumulation was done on a time step.

Results: Model verification showed a good fit of a nonlinear polynomial curve for both the measured and predicted values with R^2 values of 0.9978 to 0.9985 for zinc and 0.9978 to 0.9984 for lead at a selected time step of 15years. It was observed however, that there was an increasing tendency to uniformity of concentration with increment in the time step as a result of parameters build-up with time in the soil.

Conclusion: Finite element results revealed a high build-up in the concentration of pollutants (Zinc and Lead) in the land discharged slaughterhouses.

Keywords: Slaughterhouse, Land discharge, Finite Element Method.

1. INTRODUCTION

In Nigeria, nearly every town and neighborhood is provided with a slaughterhouse or slaughter slab. Ampofo and Awortwe (2017) [1] observed that slaughterhouses may be situated in urban, rural and nominated industrial sites, and that each has advantages and disadvantages. Simeon and Friday (2017) [2] also reported that, a cow brought for slaughtering produces 328.4kg of waste in form of dung, bone,

blood, horn and hoof. The disposal of waste products is a problem that has always dominated the slaughter sector, and on the average, 45 percent of each live beef animal, 53 per cent of each sheep, and 34 per cent of each pig consist of non-meat substances. The characteristics of slaughterhouse wastes and effluents vary from day to day depending on the number, types of stock being processed, and the processing method [3]. Clean water resources used for drinking, sustaining aquatic and terrestrial ecology, industry and aesthetic values, along with breathable air, rank as the most fundamental and important need of all viable communities. These water resources should remain within specific quality limits, and therefore require stringent and conservative protection measures. Akinnibosun and Ayejuyoni (2015)[4] reported that animal wastes can affect water, land or air qualities if proper practices of management are not adhered to. The same wastes however, can be valuable for crops but can also cause water quality impairment. It also contains organic solids, trace heavy metals, salts, bacteria, viruses, other microorganisms and sediment. The waste from animals can also be washed into streams if not protected and reduces oxygen in water, thereby endangering aquatic life. Akinnibosun and Ayejuyoni (2015)[4] also reported that improper animal waste disposal can lead to animal diseases being transmitted to humans through contact with animal feaces. Mohammed and Musa (2012), [5] reported that slaughterhouse effluents reaching streams contribute significant levels of nitrogen, phosphorous and biochemical oxygen demand, as well as other nutrients, resulting in stream pollution.

Elemile et al (2019) [6] also reported that the ground water quality in the vicinity of the slaughterhouse was adversely affected by seepage of slaughterhouse effluent as well as water quality of receiving stream that was located away from the slaughterhouse.

In virtually all the process industries and residential areas, solid and liquid wastes are generated. Slaughterhouse wastes can produce large quantities of malodorous gases when the entrained organic materials are decomposing and are allowed to settle, thereby rendering the vicinity offensive with pungent smell [4]. It also poses a danger to human health because it contains numerous pathogenic organisms removed from either the human intestinal tract or certain industrial waste. Slaughterhouse waste contains assorted nutrients that is suitable to aquatic life but may also be toxic. Due to the aforementioned reasons, immediate removal of slaughterhouse waste from the generation point, treatment and disposal is necessary.

Considering the cases of streams and rivers which receive BOD load from nearby slaughterhouses that result in deteriorating capacity of the streams, the nutrient load of these rivers were evaluated. More so, the nutrients transport within land discharged slaughterhouses were modelled using finite element approach to examine the depth and accumulation of these nutrient loads within the soil profile, hence, investigating an alternative slaughterhouse waste management mechanism. The linear finite element method was used to analyze the nutrients transport along the transverse profile of the soil using the Advective dispersive equation (ADE) as the governing equation. The equation for the stream flow pollution modelling is given as;

$$\frac{\partial c}{\partial t} + \frac{1-n}{n}\frac{\partial F}{\partial t} - \frac{\partial}{\partial x}\left(D\frac{\partial c}{\partial x} - uc\right) - \mu c \qquad (1)$$

where c is the volume averaged dispersing solute concentration in the liquid phase, F is the volume averaged dispersing solute concentration in the solid phase, D is the longitudinal dispersion coefficient (i.e. representing longitudinal dispersion), u is the unsteady uniform downward pore seepage velocity, x is the length in longitudinal direction of flow , t is time, μ is the precipitation/dissolution coefficient for solute production in the liquid phase, and n is the porosity of the different geological formations.

The Port Harcourt slaughterhouses serve the entire town, hence most of their locations beside fallow land mass have facilitated easy disposal of the wastes into soil profile without any proper treatment. This study was done to model the concentration distribution of Lead (Pb) and Zinc (Zn) along the soil strata, and also predict the accumulation level of these pollutants at selected time steps.

METHODOLOGY

2.1 STUDY AREA

Appropriate study sites were selected based on the accessibility of the location and the bench mark of long term level of pollution from slaughterhouse wastes in at least a minimum of six (6) years after a general review of various slaughterhouses was conducted within the study area. A total of three (3) slaughterhouses for land discharge were analyzed. Study area was focused on Obio Akpor and Ikwere Local Government Areas of Rivers State, with estimated population of 649,600 and 265,400 respectively all in Port Harcourt, Nigeria [9]; as shown in Figure 1.

The selected slaughterhouses evaluated are as listed below;

1) Omuigwe Slaughterhouse
2) Rukpokwu Slaughterhouse
3) Rumuekini Slaughterhouse

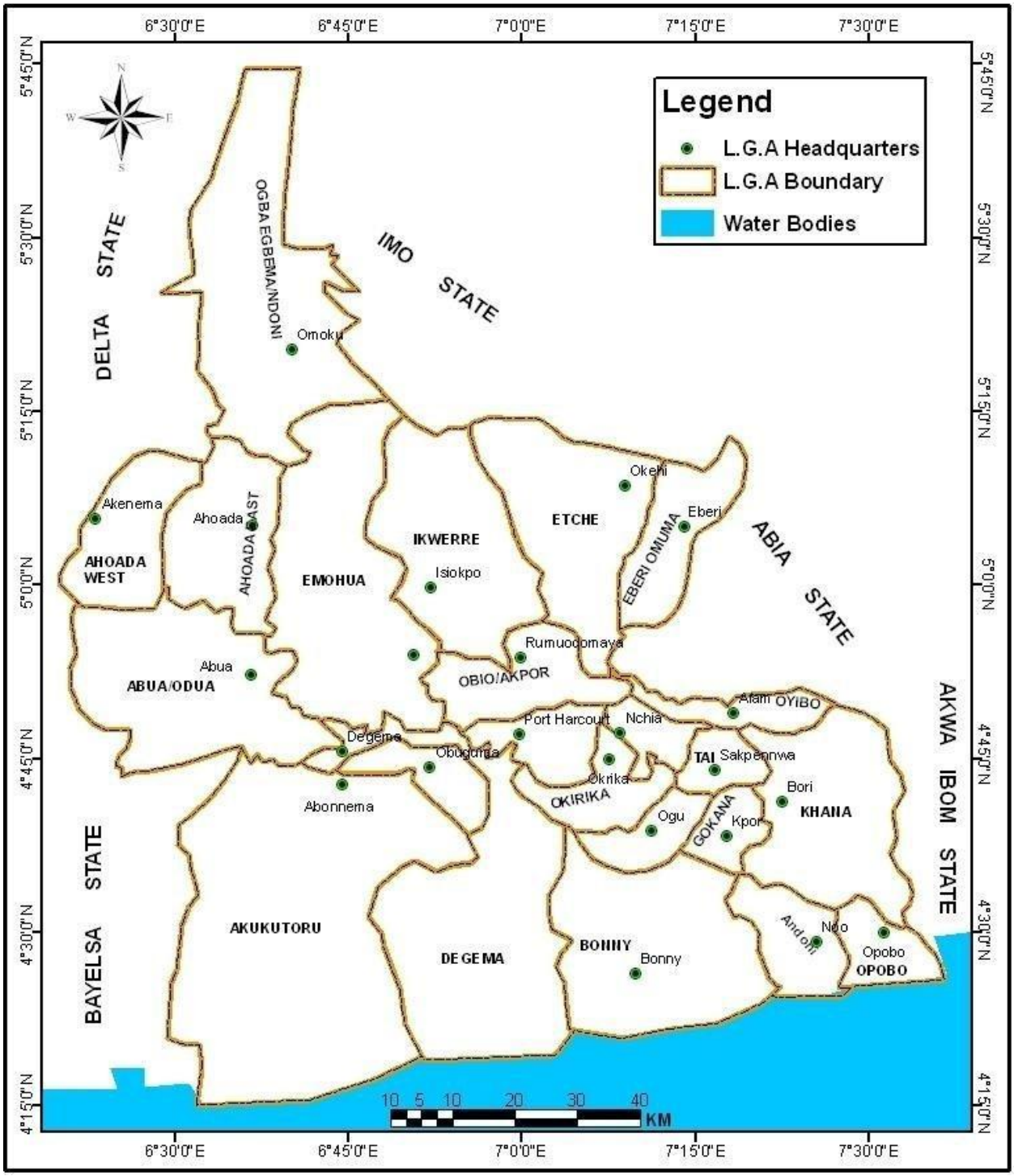

Figure 1: Map of Rivers State Showing the Local Government Areas

2.2 SAMPLE AND SAMPLING TECHNIQUES

A total of twelve composite samples were collected from three different land discharged locations. The three (is it twelve or three)composite samples each were collected from the sampling locations at a depth of 0 to 10cm, 10 to 20cm, 20 to 30cm and 30 to 40cm. Four composite samples each were collected for analysis from the three sampling locations on specified sampling dates. The samples were then placed in sterile polythene bags and transported to the laboratory for processing. Soil samples were collected from each sampling site with clean polyethylene bottles. The containers were washed with dil. HCl and then rinsed with the wastewater from the slaughterhouse so as to neutralize or reduce the effect of external contaminants. The samples were appropriately labelled and transported to the laboratory, stored in the refrigerator at 4^{o}C prior to being analyzed for the physical, chemical and biological parameters present.

2.3 NATURE AND SOURCES OF DATA

Data was strictly from laboratory analysis of the various soil parameters being considered. The soil samples were analysed for physico-chemical parameters that included: pH, turbidity, total dissolved solids (TDS), electrical conductivity (EC), total alkalinity (TA), total hardness (TH), Ca^{2+}, Mg^{2+}, Na^{+}, K^{+}, NO^{3-}, SO_4^{2-}, Cl-, Cu^{2+}, Fe^{2+} and Mn^{2+} ions. Various experimental and instrumental techniques were also employed to analyze the different chemical components.

2.4 THE DERIVATION OF THE MODEL EQUATIONS FOR CONCENTRATION

Considering a system in which non-reactive solute transport is primarily one-dimensional, i.e., solute concentrations are horizontally and vertically well-mixed so that concentrations vary only in the longitudinal or downstream direction; the effects of dispersion are constant or time-dependent with respect to distance; and the solutes are conservative in the unsteady field. Given these assumptions, the conservation of mass yields the constant parameter advection-dispersion equation (ADE) as;

$$\frac{\partial c}{\partial t} + \frac{1-n}{n}\frac{\partial F}{\partial t} - \frac{\partial}{\partial x}\left(D\frac{\partial c}{\partial x} - uc\right) - \mu c \qquad (2)$$

where c [ML^{-3}] is the volume averaged dispersing solute concentration in the liquid phase, F [ML–3]is the volume averaged dispersing solute concentration in the solid phase, D [L^2T^{-1}]is the longitudinal dispersion coefficient (i.e. representing longitudinal dispersion), u [LT^{-1}]is the unsteady uniform downward pore seepage velocity, x [L] is the length in longitudinal direction of flow , t [T] is time, μ [T^{-1}] is the precipitation/dissolution coefficient for solute production in the liquid phase, and n is the porosity of the different geological formations. A linear adsorption coefficient in terms of the solid and liquid phases is considered as

$$F = K_d C \qquad (3)$$

Where K_d is the distribution coefficient. Using equation (3) in equation (2), we have

$$R\frac{\partial c}{\partial t} - \frac{\partial}{\partial x}\left(D\frac{\partial c}{\partial x} - uc\right) - \mu c \qquad (4)$$

Where

$$R = 1 + \frac{1-n}{n}K_d \qquad (5)$$

This is the retardation factor. The retardation commonly describes a reversible sorption process, including adsorption and ion exchange. Sorption is experimentally defined by the measured quantity of a solute that

can be sorbed by a particular sediment, soil or rock. Initially the aquifer is assumed to be contaminated (i.e., some initial background concentration exists in the aquifer) and it is represented by a linear combination of some kind of initial concentration and the zero-order production term with seepage velocity.

Assuming the following assumption was considered;

i. The porous medium in is homogeneous
ii. The soil properties are constant
iii. There is no air resistance to the flow
iv. Darcy's law is valid.

The first term of the equation represents the phenomenon of diffusion and is similar to the flow equation, while the second denotes the process of transport by convection.

2.4.1 Galerkin's Finite Element Formations.

(Step 1): Presentation and selection of approximation function, a linear or quadratic shape function: N_k is chosen for that purpose and may be;

Linear shape function option.

$$\rho(x) = N_i^e C_i + N_{i+1}^e C_{i+1} = [N](c) \quad (6)$$

In which

$$N_i^e = 1 + \frac{x}{L} \quad (7)$$

and

$$N_{i+1}^e = \frac{x}{L} \quad (8)$$

are the linear shape or approximation functions of element, e, at notes i and i+1.

(Step 2): Derivation of Element Equation

The Gelarkin's weighted residual method (GWRM) is the basis of the element derivation equations of the governing equation (2). The principle is expressed mathematically as:

$$\int_R N_\beta L(\phi) dR = 0 \quad \beta = i; j, k, \ldots \quad (9)$$

Where, N_β = shape function or approximation function.

ϕ= unknown parameter and is approximated by

ϕ= [N_i, N_j, N_k,…….] [$\emptyset p$]:

$L(\phi)$= differential equation governing ϕ; and

R = region of interest.

Substituting Equation (2) into Equation (9) as follows.

$$\sum_{I}^{k-1} \int_{o}^{L} N^T \left[R\frac{\partial c}{\partial t} - \frac{\partial}{\partial x}\left(D\frac{\partial c}{\partial x} - uc \right) - \mu c \right] dx = 0 \qquad (10)$$

The second order term in Equation (10) needs to be reduced to first order equivalents using integration by parts. This transformation is necessary because of the adoption of linear shape function. Thus,

$$\sum_{I}^{K-1} \int_{0}^{L} \left[N^T R\frac{\partial c}{\partial t} - D\frac{\partial N^T}{\partial x}\frac{\partial c}{\partial x} + uN^T\frac{\partial c}{\partial x} + \mu c N^T \right] dx + D_x N^T \frac{\partial c}{\partial x}\Big|_0^L = 0 \qquad (11)$$

Thus,

$D_x N^T \frac{\partial c}{\partial x}\Big|_0^L$ can be represented as;

$$D_x N^T \frac{\partial c}{\partial x}_0^L = \left\{ D_x N_1 \frac{\partial c}{\partial x}_0^L \; D_x N_2 \frac{\partial c}{\partial x}_0^L \right\} \qquad (12)$$

We note that at $x = 0,\ N_1 = 1\ and\ N_2 = 0,\ while\ at\ x = L,\ N_1 = 0\ and\ N_2 = 1$, thus equation (12) becomes equal to;

$$D_x\{-\{\partial c\ \partial x\}1\ -\{\partial c\ \partial x\}2\} = \left\{-q_1\ q_2\right\} \qquad (13)$$

Equation (13) is known as flux vector matrix and it's interior nodes are bound to vanish during element assembly except for the end node. Thus term four will not be evaluated rather it is treated under Neumann's boundary condition in which the solutes entering the transport medium are prescribed.

Now, we substitute the discrete function $c(x) = [N]\{c\}$into equation (11) to yield;

$$\sum_{I}^{K-1} \int_{0}^{L} \left[N^T R\frac{\partial([N]\{c\})}{\partial t} - D\frac{\partial N^T}{\partial x}\frac{\partial([N]\{c\})}{\partial x} + uN^T\frac{\partial([N]\{c\})}{\partial x} + \mu c N^T \right] dx = 0 \qquad (14)$$

2.4.2 Element Formulation with Linear Shape Function

Term 1:

$$\int_0^L N^T R\frac{\partial([N]\{c\})}{\partial t} dx = \int_0^L RN^T\frac{\partial c}{\partial t} dx = \int_0^L \left[\left[1 - \frac{x}{L}\right]\frac{x}{L}\right]\left[\left(1 - \frac{x}{L}\right)\frac{x}{L}\right]\left\{\dot{c}_1\ \dot{c}_2\right\} dx$$

$$= \frac{RL}{6}[2\ 1\ 1\ 2]\left\{\dot{c}_1\ \dot{c}_2\right\} \qquad (15)$$

Where $\dot{c} = \frac{\partial B}{\partial t}$; time derivative of c.

Term 2:

$$\int_O^L D_x \frac{\partial N^T}{\partial x} \frac{\partial([N]\{c\})}{\partial x} = \int_O^L \frac{D_x}{L} \{-\ 1\ 1\} \frac{1}{L} [-\ 1\ \ 1] \left[c_1\ c_2\right] dy$$

$$= \frac{D_x}{L} [-\ 1\ 1\ \ -\ 1\ 1] \left[c_1\ c_2\right] \quad (16)$$

Term 3:

$$\int_0^L u N^T \frac{\partial([N]\{c\})}{\partial x} dx = \int_O^L u \left[\left[1 - \frac{x}{L}\right] \frac{x}{L}\right] \frac{1}{L} [-\ 1\ \ 1] \left[c_1\ c_2\right] dy$$

$$= \frac{u}{2} [-\ 1\ 1\ \ -\ 1\ 1] \left[c_1\ c_2\right] \quad (17)$$

Term 4:

$$\int_O^L \mu N^T \partial y = \int_O^L \mu \left[(1 - \frac{x}{L)}\ \frac{x}{L}\right] dy = \frac{\mu L}{2} [1\ 1] \quad (18)$$

As stated earlier term five is known as flux vector matrix and its interior nodes are bound to vanish during element assembly except for the end nodes. Thus combining each of the evaluation terms yields the following element equations:

$$\frac{RL}{6} [2\ 1\ 1\ 2] \left\{\dot{c}_1\ \dot{c}_2\right\} - \frac{D_x}{L} [-\ 1\ 1\ \ -\ 1\ 1] \left[c_1\ c_2\right] + \frac{u}{2} [-\ 1\ 1\ \ -\ 1\ 1] \left[c_1\ c_2\right] + \frac{\mu L}{2} [1\ 1] = 0 \quad (19)$$

Equation (19) if rearranged generates, Equation (20) as stated below;

$$\frac{RL}{6} [2\ 1\ 1\ 2] \left\{\dot{c}_1\ \dot{c}_2\right\} - \frac{D_x}{L} [-\ 1\ 1\ \ -\ 1\ 1] \left[c_1\ c_2\right] + \frac{u}{2} [-\ 1\ 1\ \ -\ 1\ 1] \left[c_1\ c_2\right] = -\frac{\mu L}{2} [1\ 1] \quad (20)$$

2.4.3 Assembling of Element Equations into a Global Equation

We assume a one-dimensional stretch, divided into three elements with four nodes (linear option) see Figure (2).

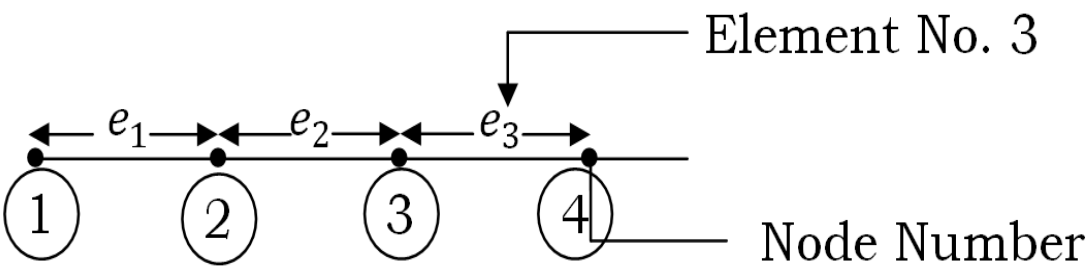

Figure 2: Discretized one-dimensional linear option stretch

The assembled global matrix equation of Equation (20) can assume the following general form;

$$[A]\{\dot{c}\} + [E]\{c\} = \{F\} \quad (21)$$

In which $[A]$ is the assemblage of the first matrix; $[E]$ is obtained by the addition of the assemblage of the second and third matrix and $\{F\}$ is the assemblage of the flux vector (Fourth term), respectively.

Because of the time derivative $\{\dot{c}\}$in equation (21), there is a need to conduct some form of approximation to the derivatives to reduce the equation to a system of algebraic equivalent.

2.4.5 Approximation of Time Derivatives

This involves the process of regarding the basis or approximation function as being dependent on time as well as the domain. A better approach to the time derivative approximation is the semi discrete method in which the time derivation of a variable at node is represented by a temporal operator (Finite Difference operator) from the relationship as shown below;

$$\frac{\partial c(x,t)}{\partial t} = \dot{c}_i(x,t) = N_i(x)\dot{c}_i(t) \quad (22)$$

Where $\dot{c}_i(t)$ is the time derivative of c prescribed at node, i (to be approximated using finite difference scheme).

Using the forward in time (implicit) scheme where forward difference is represented as;

$$\dot{C} = \frac{C^{K-1} - C^K}{\Delta t} \quad (23)$$

As $K = time\ level$

Substituting Equation (23) into Equation (21) yields;

$$[A]\left\{\frac{C^{K-1} - C^K}{\Delta t}\right\} + [E]\{c\} = \{F\} \quad (24)$$

For Equation (3.23) an implicit equation is possible with the aid of the time weighting factor.

The works of Nwaogazie on mass transport modelling shows that the value of dimensionless time-weighting factor $\theta = 0.55$ minimized distortion while conservatively ensuring theoretical stability criteria.

The tendency for the stability of the numerical computations to decrease with increasing values of θ exists.

As stated by Nwaogazie (2008) the introduction of the dimensionless time-weighting factor, θ to Equation (21) results as follows;

$$[A + \Delta t\theta E\}\{C\}^{K+1} = [A - \Delta t(1 - \theta)E\}\{C\}^{K} + [F]^{K} \quad (25)$$

Where $\Delta t = time\ step\ and\ \theta = time - weighting\ factor$. If $\theta = 0$ Equation (25) becomes an explicit model; whereas $\theta = 0.5\ or\ 1.0$ results in Crank Nicholeon Formulation or fully implicit model respectively. From the experience of various researchers $\theta - values\ of\ 0.55\ to\ 1$ yields stable solutions. However a conservative value of 0.55 produces the least or near zero numerical dispersion and thus, it is so recommended for use (Nwoagazie , 2008).

$$\left(\frac{RL}{6}[2\ 1\ 0\ 0\ \ 1\ 4\ 1\ 0\ \ 0\ 0\ \ 1\ 0\ \ 4\ 1\ \ 1\ 2\ \ ] + \Delta t\theta\left[e_1 + e_2\ \ - e_1 - e_1\ \ \ - e_1 + e_2\ 2e_1\ \ - e_1 - e_2\ \ \ \ - e_1 + e_2\ \ 2e_1\ \ - e_1 - e_2\ \ -\right.\right.$$

Where; $e_1 = \frac{D_x}{L}$, $e_2 = \frac{u}{2}$, $K\ and\ K + 1$ represent initial conditions, at $t = 0$ and first-time level, respectively.

3.7.5 Model Resolution

Parameters for the model calculation are as highlighted below;

C is the volume averaged dispersing solute concentration in the liquid phase (To be evaluated)

D_x is the longitudinal dispersion coefficient $= 0.628\frac{m^2}{year}$

Which was determined experimentally using Equation (27) as stated below;

$$D_x = \frac{M^2\pi}{4\theta^2C^2t} \quad (27)$$

Where $M =$ the initial amount of parameter determined (e.g., Lead from source), $C =$ concentration at a distance after dispersion over time ($\frac{g}{cm^3}$), $\theta =$ moisture content of the soil, $\pi = 3.142$, and $t =$ corresponding time interval (Seconds or hours)

u is the unsteady uniform downward pore seepage velocity$= 0.4111\frac{m}{year}$

μ is the average mean precipitation/ dissolution solvent per year (the model Sink/Source factor) $= 200.45\frac{mm}{year} = 0.20025\frac{m}{year}$

R is the retarding factor as expressed below;

$$R = 1 + \frac{1-n}{n}K_d \quad (28)$$

$K_d = distribution\ coefficient = 1.6772$ as determined experimentally.

Substitution of K_d and n into Equation 3.27 generates R as shown below;

$$R = 1 + \frac{1-0.50625}{0.50625}1.6772 = 2.6358$$

θ is the dimensionless time-weighting factor $= 0.55$

Δt is the time step $= 3\ years$

Therefore;

$$e_1 = \frac{D_x}{L} = \frac{0.628}{1} = 0.628$$

$$e_2 = \frac{u}{2} = \frac{0.4111}{2} = 0.20555$$

$$\frac{RL}{6} = \frac{2.6353\times1}{6} = 0.4393$$

$$\frac{\mu L}{2} = \frac{0.20045\times1}{2} = 0.100225$$

$$\Delta t(1 - \theta) = 3(1 - 0.55) = 1.35$$

$$\Delta t(\theta) = 3(0.55) = 1.65$$

The governing differential equation for concentration given as equation (3.2) is subject to the following conditions for evaluation:

$$R\frac{\partial c}{\partial t} = \frac{\partial}{\partial x}\left(D\frac{\partial c}{\partial x} - uc\right) - \mu c$$

$$C(0,t) = C_1,\ t > 0$$

$$C(\infty,t) = 0,\ t > 0$$

$$C(y,0) = C_0,\ y \geq$$

Where,

C_1 is the input concentration

C_0 is the initial concentration of the solute in the fluid.

3.0 RESULTS AND DISCUSSION

3.1 Finite Element Model Result Analysis

Results of the finite element model as shown in Figures 3 to 8, established that the concentration of pollutants decreases with an increase in the nodal points (depth of soil) at different time steps.

3.1.1 Finite Element Model plot for Zinc Concentration Distribution at Varying Nodal Points

A graphical plot of Zinc concentration distribution at Varying Time Steps is as shown in Figure 3.

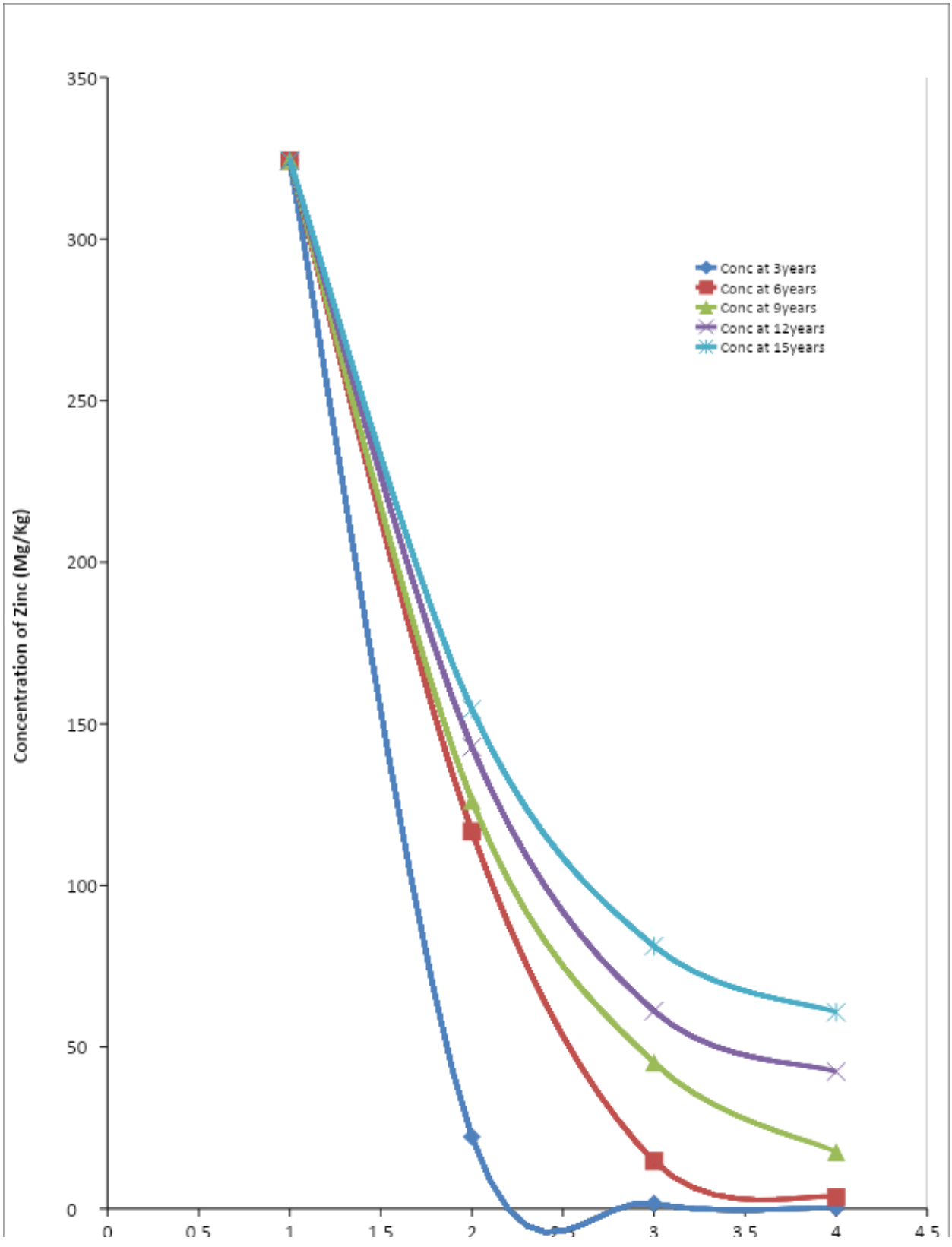

Figure 3: Graphical plot of Zinc concentration at Varying Time Steps.

Also, model result of zinc concentration distribution at the different nodal points observed are as shown in Figures 4 and 5.

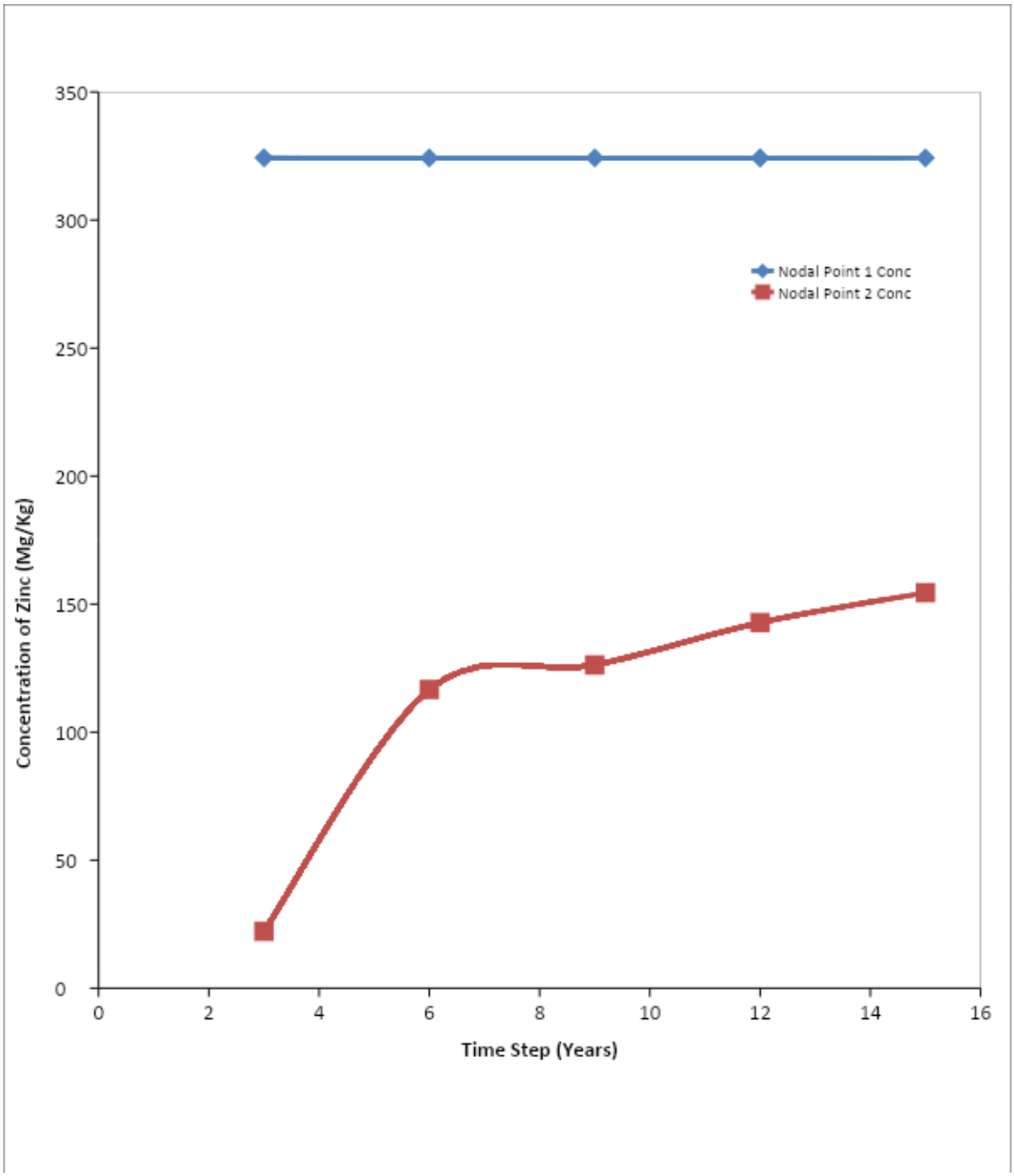

Figure 4: Zinc Concentration at Nodal points 1 and 2.

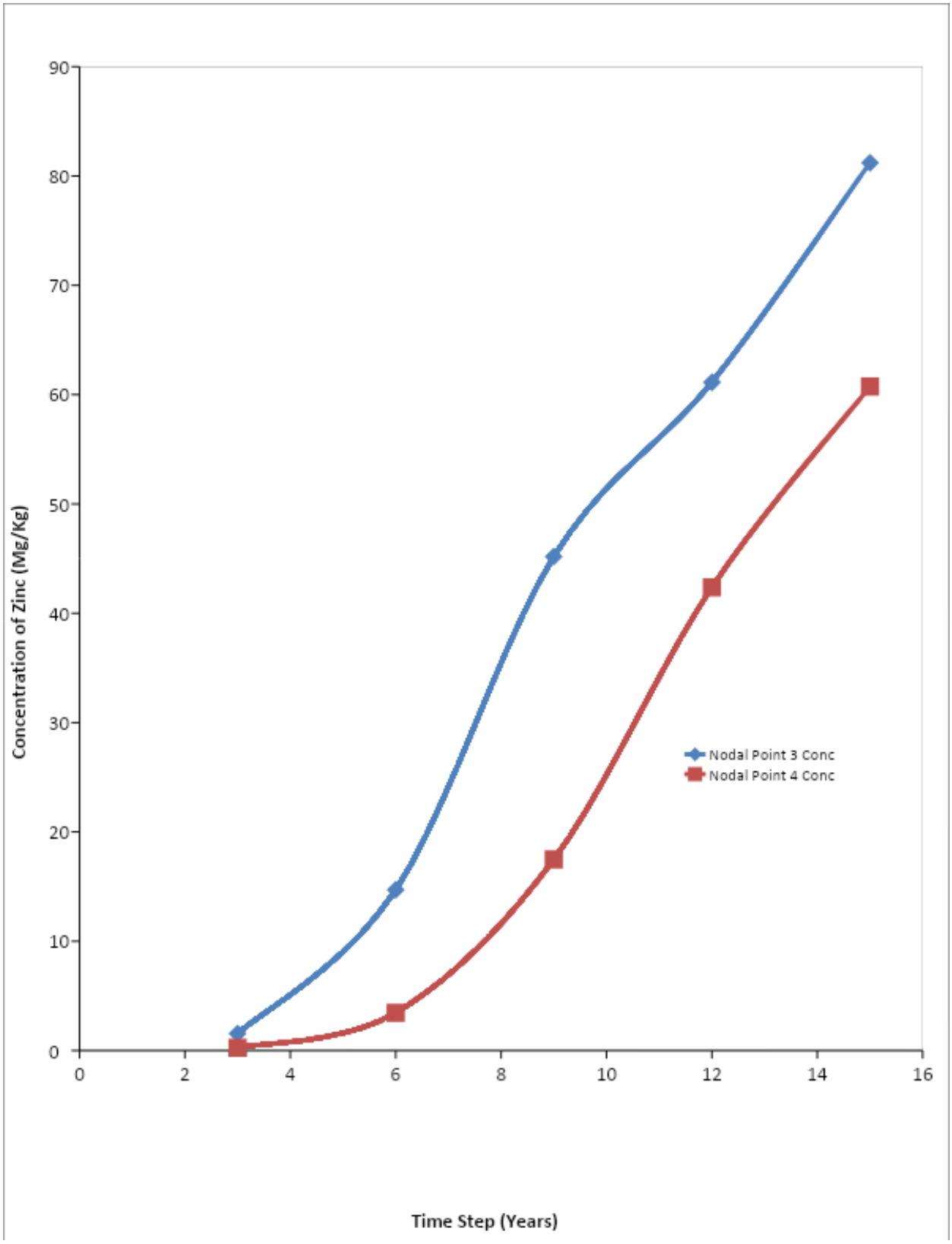

Figure 5: Zinc Concentration at Nodal points 3 and 4

3.1.2 Finite Element Model plot for Lead Concentration Distribution at Varying Nodal Points

On a similar view, the graphical plot of Lead concentration distribution at Varying Time Steps is as shown in Figure 6.

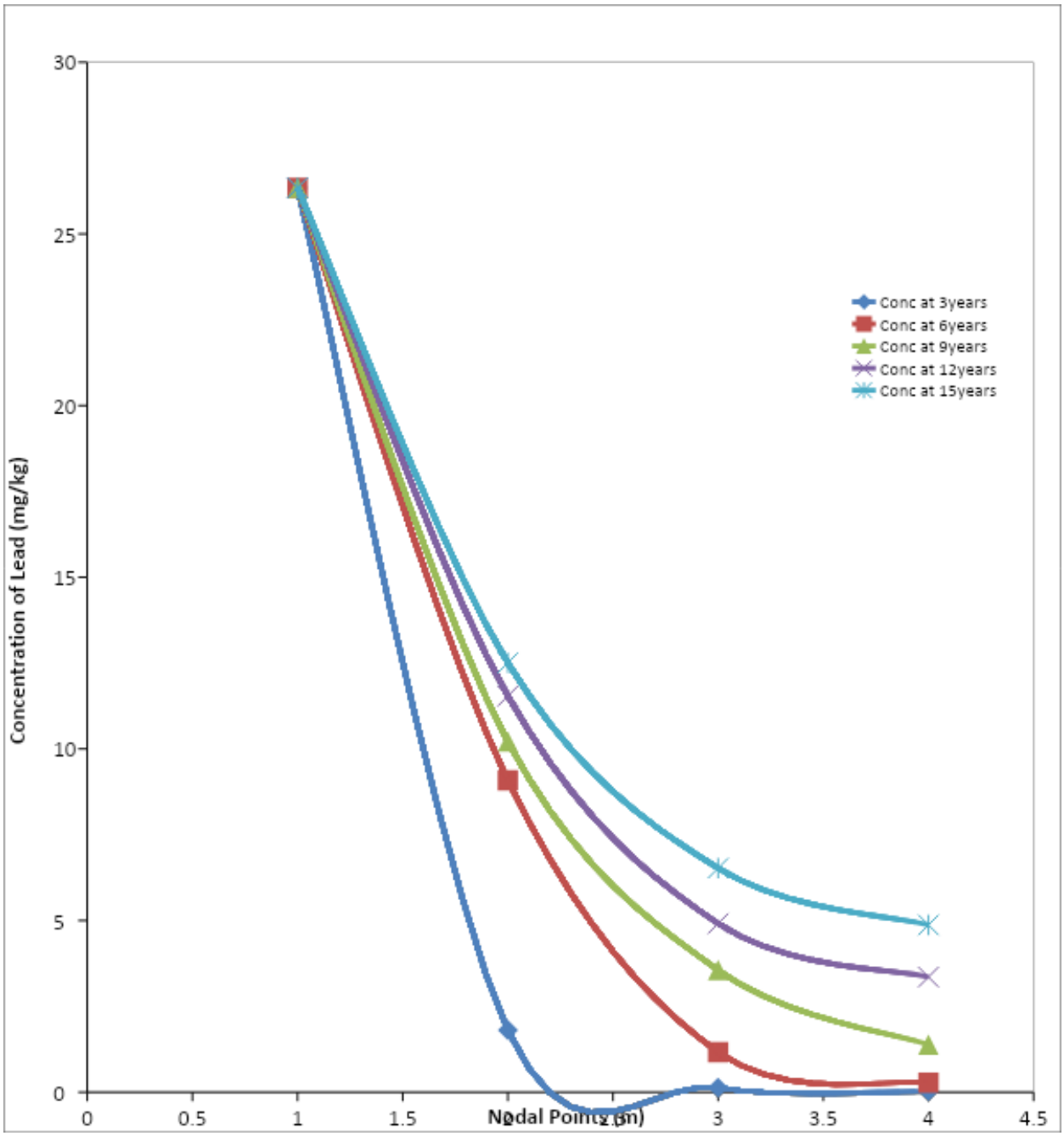

Figure 6: Graphical plot of Lead concentration at Varying Time Step

Also, model result of Lead concentration distribution at the different nodal points observed are as shown in Figures 7 and 8.

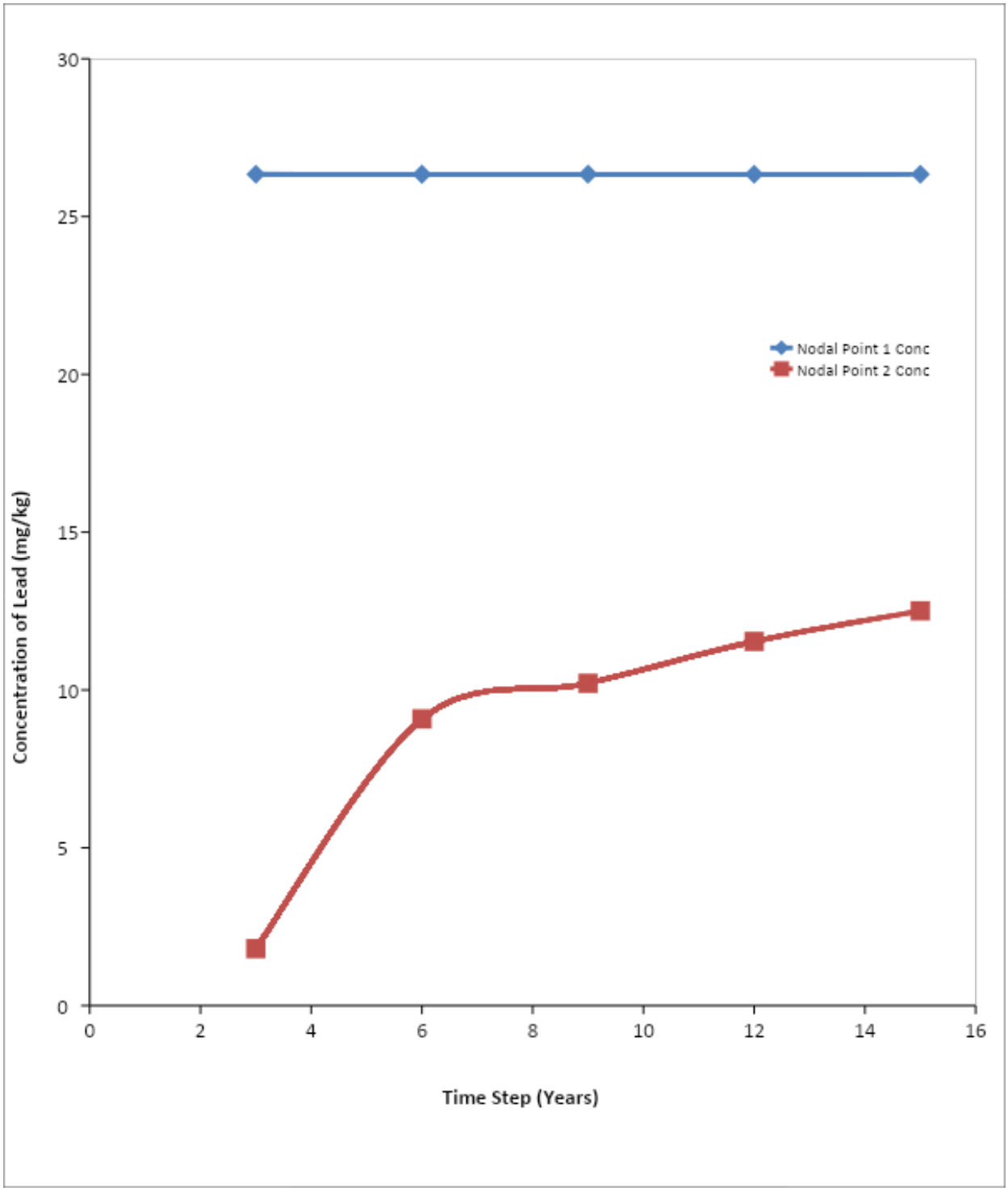

Figure 7: Lead Concentration at Nodal points 1 and 2.

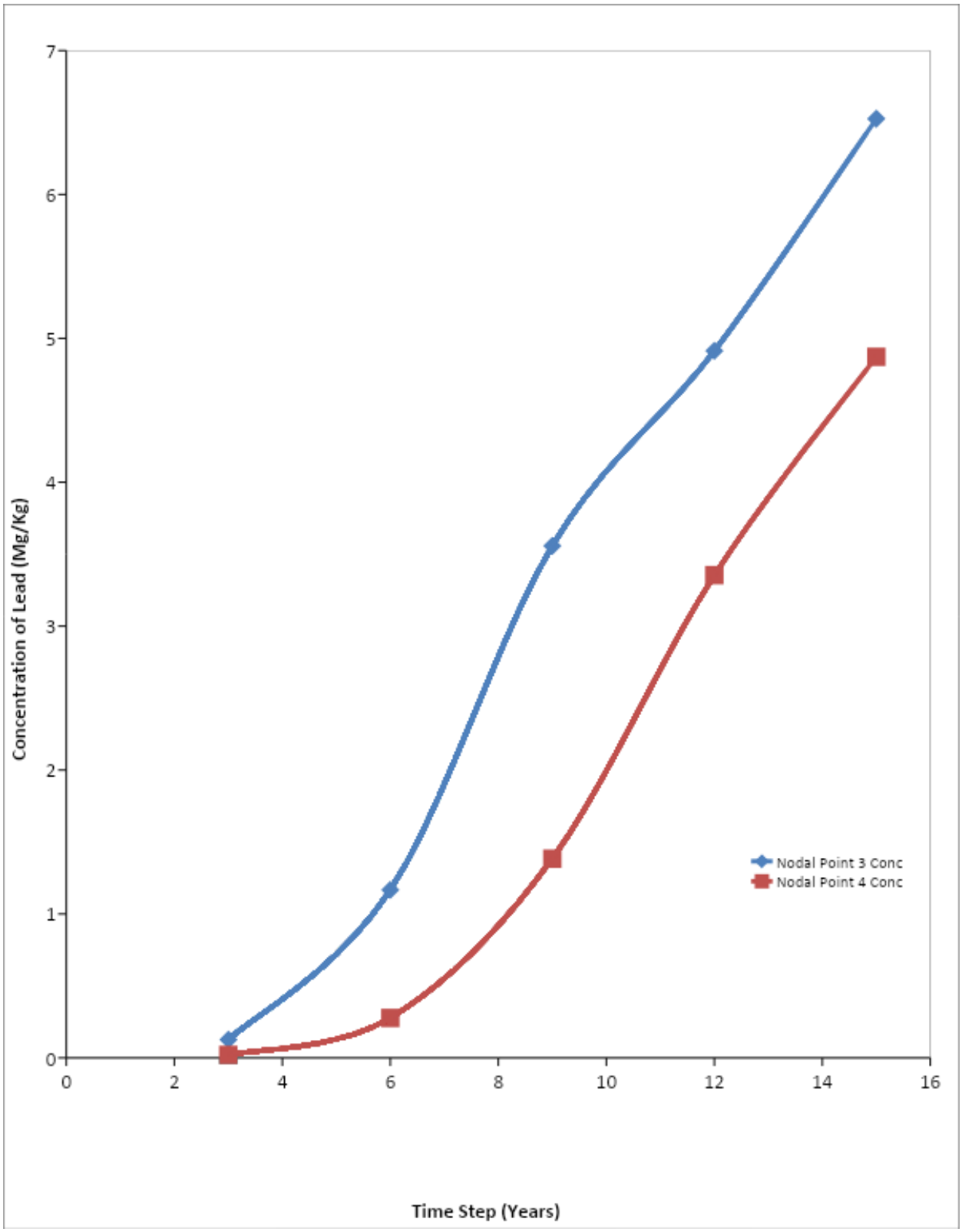

Figure 8: Lead Concentration at Nodal points 3 and 4.

4.1.4 Model Verification Using Concentration Fitted Data

From the measured laboratory data obtained during sampling, the concentration of Zinc and Lead at different nodal points with a time step interval of 3years were calculated. The experimental representation of concentration was determined using the global assembled finite element equation (26) and relevant experimental data. Hence, a nonlinear regression predicted data at different nodal points and time steps, generated a close polynomial curve fitting as the model generated data curve, with R^2 value ranges of 0.9978 to 0.9985 for Zinc and 0.9978 to 0.9984 for Lead at an iteration time step of 15years respectively as shown in Figures 9 and 10.

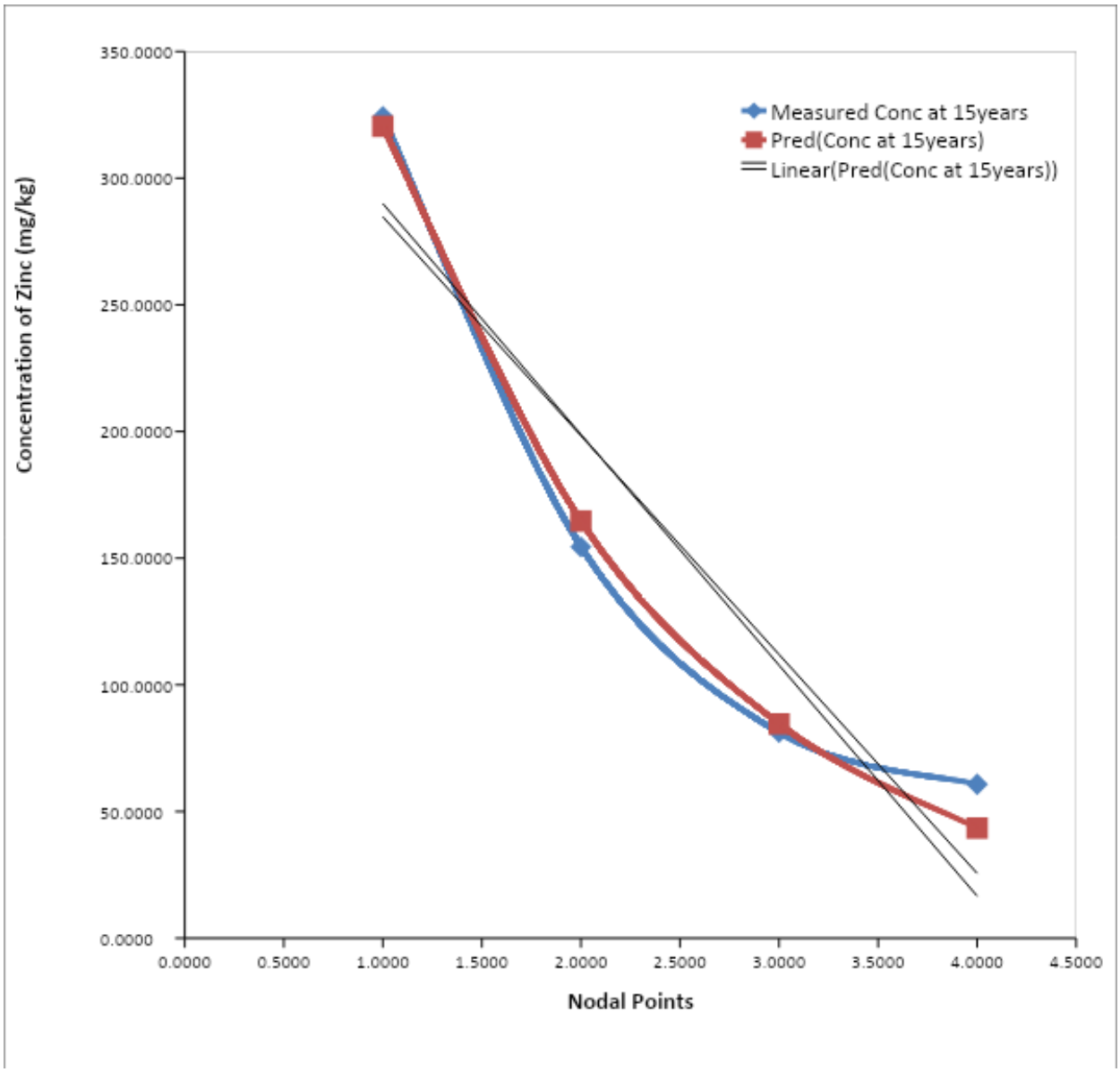

Figure 9: Zinc Concentration versus Nodal point Plot of Measured and Predicted Data for Nonlinear Regression at 15years time step

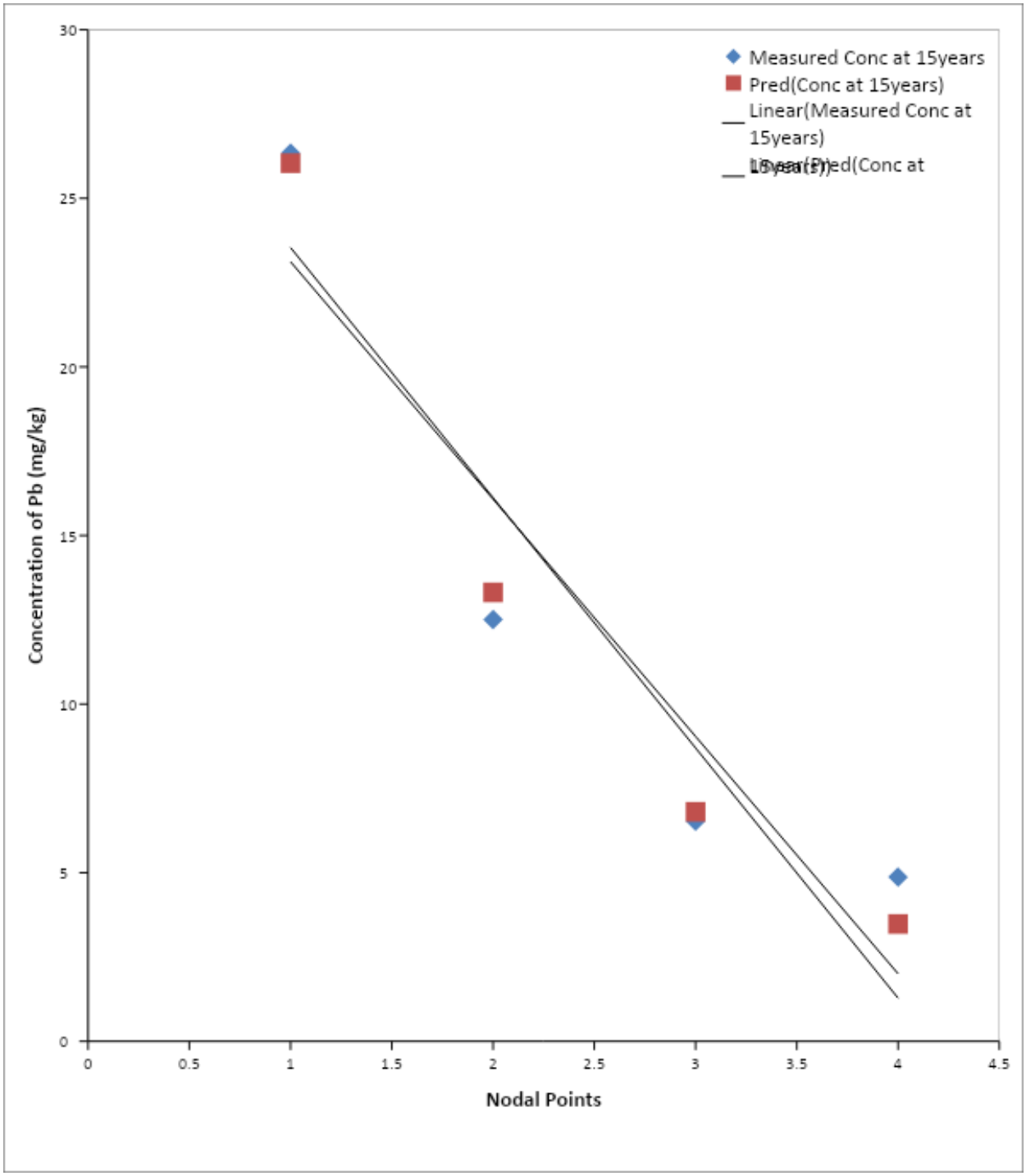

Figure 10: Lead Concentration versus Nodal Points Plot of Measured and Predicted Data for Nonlinear Regression at 15 year time step.

3.2 FINITE ELEMENT MODEL ANALYSIS

Model result for the concentration of Zinc at varying time steps show an increased amount as the time of the year increased. The actual concentration of Zinc decreased as the depth of the soil increased, however, a close look at the trend of concentration plot shows that there was a gradual increase in concentration as the time step increased as shown in Figure 3.

A critical look at the concentration of Zinc at specified nodal points shows a large margin between the concentrations at node 1 as compared to node 2. Node 1 being the top surface of the soil tends to assume a uniform /highest concentration at an experimented depth of 0-10 cm. As the depth of pollutant transport gets deeper at node 2, variational trend of zinc concentration tends to an irregular curve as a result of the variations in the pore spaces of the soil (Kumar and Singh, 2019) as shown in Figure 4.

Continuous observation of the model result shows that at nodal points 3 and 4, the variational curve of zinc concentration tends to become uniform, hence showing a similar trend of curve, which can be described as a patterned flow of zinc concentration build-up as shown in Figure 4.15 from the uniform denser packed pore spaces from pressure of topsoil weight and activities of humans on the topsoil (Chen et al, 2016).

On a similar view, model results for the concentration of Lead at varying time steps show an increased amount as the time of the year increased. The actual concentration of lead decreased as the depth of the soil increased; however, a close look at the trend of concentration plot shows that there was a gradual increase in concentration as the time step increased as shown in Figure 6.

Similarly, a critical look at the concentration of Lead at specified nodal points shows that there is a large margin between the concentrations at node 1 as compared to node 2. Node 1 being the top surface of the soil tends to assume a uniform /highest concentration at an experimented depth of 0-10 cm. As the depth of pollutant transport gets deeper at node 2, variational trend of Lead concentration tends to an irregular curve as a result of the variations in the pore spaces of the soil as shown in Figure 7.

Continuous observation of the model result shows that at nodal points 3 and 4, the variational curve of Lead concentration tends to become uniform, hence showing a similar trend of curve, which can be described as a patterned flow of Lead concentration build-up as shown in Figure 8 from the uniform denser packed pore spaces from pressure of topsoil weight and activities of humans on the topsoil.

4. CONCLUSION

The increase in concentration at lower depths observed may be explained thus: during filtration, each particle moved separately from one another and easily followed the streamlines of flow directed towards the pore in the filter medium. The results indicated that a particle, depending on the ratio of pore diameter of the filter medium to particle diameter will either enter a pore or will cover the pore opening, resulting in blockage of the pore and the filter causing an increase to the resistance to flow through the filter.

However, as the time increased, the concentrations also showed an increase at different depths of the soil profile, resulting from a build-up of pollutants/nutrients within a specified period of time. The plot of concentration versus nodal points given indicated a pronounced increase of pollutants/ nutrients in the

soil profile as the year progressed. This further explained the tendency of concentration being uniform as the time of accumulation increased.

REFERENCES

1. Ampofo E. A. and Awortwe D. (2017): Heavy metal (Cu, Fe and Zn) pollution in soils: pig waste contribution in the Central Region of Ghana. Adv Appl Sci Res;8:1-10.
2. Simeon E. O. and Friday K. (2017): Index models assessment of heavy metal pollution in soils within selected slaughterhouses in Port Harcourt, Rivers State, Nigeria. Singapore J Sci Res;7:9-15.
3. Abubakar G. A. and Tukur A. (2014): Impact of slaughterhouse effluent on soil chemical properties in Yola, Adamawa State, Nigeria. Int J Sustain Agricult Res;1:100-107.
4. Akinnibosun F. I and Ayejuyoni T. P. (2015): Assessment of microbial population and physico-chemical properties of slaughterhouse effluent-contaminated soils in Benin City, Nigeria. Journal of Tropical Agricult Food Environ Exten;14:1-6.
5. Mohammed S. and Musa J. J. (2012). Impact of Slaughterhouse Effluent on River Landzu, Bida, Nigeria. J. Chem. Biol. Phys. Sci. 2(1), 132-136.
6. Ediene V. F; Iren O. B and Idiong M.M. (2016): Effects of slaughterhouse effluent on the physicochemical properties of surrounding soils in Calabar Metropolis. Int J Adv Res;4:37-41.
7. Elemile O. O., Raphael D. O., Omole D.O., Oloruntoba E. O., Ajayi E.O. and Ohwavborua N. A. (2019): Assessment of the impact of slaughterhouse effluent the quality of groundwater in a residential area of Omu-Aran, Nigeria. Environ Sci Europ;31:1-10.
8. Nwaogazie, I. L. (2008). Finite element modeling of engineering systems. 2nd edition, Special publishers, Enugu. Pp 115-135
9. Kumar, P. and Singh, A. (2019); Groundwater Contaminant Transport Modelling for Unsaturated Media using Numerical Methods (FEM, FDM). Int. J. Recent Technol. Eng. (IJRTE), 8, 2277–3878.(7)
10. Chen, C.S.; Tu, C.H.; Chen, S.J. and Chen, C.C. (2016); Simulation of Groundwater Contaminant Transport at a Decommissioned Landfill Site-A Case Study, Tainan City, Taiwan. Int. J. Environ. Res. Public Health. 13, 467. [CrossRef]